[CANCER RESEARCH 61, 6811–6815, September 15, 2001]

The Susceptibility of Tumors to the Antivascular Drug Combretastatin A4 Phosphate Correlates with Vascular Permeability[1]

Daniel A. Beauregard, Sally A. Hill, Dai J. Chaplin, and Kevin M. Brindle[2]

Department of Biochemistry, University of Cambridge, Cambridge CB2 1GA [D. A. B., K. M. B.], and Gray Laboratory Cancer Research Trust, Mount Vernon Hospital, Northwood, Middlesex HA6 2JR [S. A. H., D. J. C.], United Kingdom

ABSTRACT

The acute effects of the antivascular drug, combretastatin A4 phosphate, on tumor energy status and perfusion were assessed using magnetic resonance imaging (MRI) and spectroscopy. Localized ^{31}P magnetic resonance spectroscopy showed that LoVo and RIF-1 tumors responded well to drug treatment, with significant increases in the P_i/nucleoside triphosphate ratio within 3 h, whereas SaS, SaF, and HT29 tumors did not respond to the same extent. This variable response was also seen in MRI experiments in which tumor perfusion was assessed by monitoring the kinetics of inflow of the contrast agent, gadolinium diethylenetriaminepentaacetate. These data were analyzed to give the initial rate and time constant for inflow of contrast agent and the integral under the inflow curve. The differential susceptibility of the tumors to combretastatin A4 phosphate showed a positive correlation with prior MRI measurements of tumor vascular permeability, which was determined by measuring the inflow of a macromolecular contrast agent, BSA-gadolinium diethylenetriaminepentaacetate.

INTRODUCTION

The tubulin-binding drug combretastatin A4, originally isolated from the southern African willow, *Combretum caffrum* (1), has been shown to be effective in disrupting the vasculature of tumor models at concentrations well below the maximum tolerated dose (2). Phase I clinical trials of CA4P,[3] which is converted to combretastatin A4 by nonspecific endogenous phosphatases, are currently underway (3). Combretastatin A4 initiates apoptotic death of proliferating, but not quiescent, endothelial cells (4). However, disruption to blood supply in tumor models is seen within ~20 min (2, 5), and it appears unlikely that this is attributable either to apoptosis of endothelial cells or to antimitotic effects of CA4P, both of which would be likely to exert their effects over a longer timescale. CA4P induces a rapid change in shape in recently divided endothelial cells (2), and it may be this which triggers vascular disruption and hemorrhage leading to the death of tumor cells as a secondary event. Low levels of NO have been shown to potentiate the vascular damage induced in tumors by CA4P (6, 7). A reversible increase in vascular resistance is seen in several tissues including spleen, heart, and kidney, after CA4P treatment, but the effects are more marked and, at sufficiently high doses, irreversible in tumors. This may be because tumor vessels are poorly developed and because the tumor interstitial fluid pressure is high (7, 8). However, even in those cases where vascular damage induces extensive necrosis, a rim of viable cells can remain at the tumor periphery, from which the tumor can continue to grow, with little effect on growth rate (9). For this reason, it has been suggested that antivascular therapies should be combined with conventional therapies, *e.g.*, combination therapy of cisplatin with CA4P has been used to eliminate the viable tumor cells that remain at the tumor periphery following CA4P treatment (9).

Because CA4P treatment has little effect on tumor growth rate, the action of the drug cannot be detected simply by monitoring tumor volume. For this reason, we implemented noninvasive MRI and MRS experiments to determine the effect of the drug on perfusion in a murine tumor model (5). Similar MRI experiments are now being used to assess patient response in a Phase I clinical trial (10). In our earlier study, dynamic inflow experiments with the contrast-enhancing agent GdDTPA indicated that response of the sarcoma F tumor to CA4P was spatially heterogeneous, with some regions showing very large decreases in perfusion. This heterogeneity may be explained by the angiogenic "hot spots" that exist around necrotic regions of tumors and which indicate a heterogeneous distribution of growth factors (11) and, hence, dividing endothelial cells, which may therefore be combretastatin sensitive. In many tumors, the main growth factor involved in stimulating division of endothelial cells is VEGF, which also causes increased vessel permeability (8). MRI experiments with macromolecular contrast agents like BSA-GdDTPA have been used to identify regions of permeable vasculature within tumors, which may be used as a surrogate marker for VEGF expression (12–17). Noninvasive MRI and MRS experiments have been used here to map the permeability of vessels in five tumor models in mice and to determine whether there is a correlation with tumor susceptibility to CA4P.

MATERIALS AND METHODS

Tumor Models. Five transplanted tumor models were used in this study, initiated by s.c. injection of a tumor cell suspension (10^5 cells) dorsally into 10–16-week-old female mice. Two of the models were human colon adenocarcinomas xenotransplanted in SCID mice: HT29 and LoVo; the cell lines were obtained from the American Type Culture Collection. Three of the models were murine: radiation-induced fibrosarcoma (RIF-1; Ref. 18) implanted in C3H and SCID mice and SaS and SaF (19) implanted in CBA mice. SaS is a slow growing, poorly differentiated, round-celled sarcoma, and SaF is a rapidly growing anaplastic sarcoma. These tumors arose spontaneously in CBA mouse colonies at the Gray Laboratory in 1962 and 1957, respectively. All data are given from $n = 6$ experiments with each tumor type. The experiments were conducted when tumors reached ~10-mm geometric mean diameter; this was 11–16 days (RIF-1 and SaF), 20–30 days (HT29), or 50–60 days (LoVo and SaS) after implantation. Studies were conducted in accordance with a project license issued under the United Kingdom Animals (Scientific Procedures) Act 1986.

Anesthetic, CA4P, and Contrast Agent Preparation. Anesthesia was induced before beginning the experiments (3.9 mg/kg fentanyl citrate + 125 mg/kg fluanisone + 50 mg/kg midazolam, i.p.) and then maintained throughout (0.2 mg/kg fentanyl citrate + 6.7 mg/kg fluanisone, i.p. every 1.75 h). Animals were placed in a cradle, which held the tumor in the center of the surface coil used for tumor imaging and spectroscopy. A flow of warm air was used to maintain the body temperature. Combretastatin A4, as the disodium combretastatin A4 3-*O*-phosphate prodrug (kindly provided by G. R. Pettit, Arizona State University, Tempe, AZ; Ref. 20), was dissolved in sterile saline (0.9% NaCl) and injected i.p. to give 100 mg/kg body weight. BSA-GdDTPA, prepared as described by Ogan *et al.* (21), was administered i.v. through a tail-vein catheter over a period of 30 s, to give 250 mg/kg body weight. GdDTPA (Magnevist, Schering, United Kingdom) was administered i.v.

Received 11/27/00; accepted 7/18/01.

The costs of publication of this article were defrayed in part by the payment of page charges. This article must therefore be hereby marked *advertisement* in accordance with 18 U.S.C. Section 1734 solely to indicate this fact.

[1] Supported by the Cancer Research Campaign (Project Grant SP2350/0101).

[2] To whom requests for reprints should be addressed, at Department of Biochemistry, University of Cambridge, Tennis Court Road, Cambridge CB2 1GA, United Kingdom.

[3] The abbreviations used are: CA4P, combretastatin A4 phosphate; MRI, magnetic resonance imaging; MRS, magnetic resonance spectroscopy; GdDTPA, gadolinium diethylenetriaminepentaacetate; NTP, nucleoside triphosphate; VEGF, vascular endothelial growth factor; SCID, severe combined immunodeficient.

through a tail-vein catheter over a period of 30 s, to give 188 mg/kg body weight.

MRI and MRS. Experiments were performed in a 9.4 T vertical-bore (8.9-cm diameter) superconducting magnet (Oxford), interfaced with a Varian UnityPlus spectrometer. An unshielded gradient set (Varian) was used with a probe incorporating a two-turn surface coil (20-mm diameter) tunable to frequencies of 400 MHz (^{1}H imaging) and 162 MHz (^{31}P spectroscopy). Data were processed using VNMR 5.3 and Image Browser 6.1 software (both Varian) and software written in C in this laboratory.

Contrast Agent Inflow Experiments. BSA-GdDTPA or GdDTPA were introduced over 30 s as a bolus via a tail-vein catheter, and inflow into the tumor was monitored with a series of T_1-weighted spin-echo images (TE = 12.3 ms, TR = 130 ms), which were collected for ~15 min postinjection. For calculation of the paramagnetic contribution to the longitudinal relaxation rate (R_{1p}) from the GdDTPA inflow experiments, an image with TR = 3 s was also acquired (22). Images were acquired from a 1-mm thick slice, and the field of view was 20 mm over a 256 × 128 (phase encode) matrix, which was zero-filled to 256 × 256 data points. BSA-GdDTPA inflow experiments were made before treatment with CA4P. Measurements of Gd-DPTA inflow and washout were carried out on the same animals before treatment with CA4P and 3 h after treatment. The animal was anesthetized throughout this period. Because BSA-GdDTPA concentration in the blood decreases monoexponentially with a half-life of 3 h (23, 24), it was assumed that there were no changes in signal intensity because of changes in concentration of BSA-GdDTPA during the subsequent GdDTPA inflow experiments. The GdDTPA inflow experiment at 3 h was not compromised by the earlier experiment as image intensities returned to baseline levels within ~2 h after the first GdDTPA injection. For the range of tissue concentrations of GdDTPA used in the study, the concentration was linearly proportional to relaxivity (data from phantom studies not shown).

Analysis of BSA-GdDTPA Inflow Data. Vascular permeability was determined according to the pharmacokinetic model described by Su *et al.* (25), in which the signal intensity in each pixel depends on the concentration of contrast agent in the plasma (C_p) and tumor interstitial (C_i) volume fractions (V_p and V_i). The time dependencies of these concentrations are governed by transport constants from the plasma compartment to the interstitial compartment (K_1) and *vice versa* (K_2). We made several assumptions which simplified the analysis of our data. The initial concentration of contrast agent in the plasma was assumed to be reached at the time of injection. The concentration of contrast agent in the plasma, C_p, was assumed to remain constant during the course of the experiment, because the half-life for clearance is 3 h (23, 24). As others have done (24), we assume that for experiments of this duration using BSA-GdDTPA, the transport constant from the extracellular compartment to plasma, K_2, is zero. Indeed, we were not able to obtain values for K_2 because the relatively low concentrations of BSA-GdDTPA achieved in the extracellular compartment did not permit an accurate determination. Experimental data were fit to a consequently simplified version of Su *et al.*'s model, shown in Eq. 1, where $D_0 = V_pC_p$ and $D_1 = V_iC_pK_1$; C_T is the total concentration of contrast agent in a given pixel:

$$C_T(t) = D_0 + D_1t \quad \text{(A)}$$

A calibration curve relating signal intensity (S) under our experimental conditions to BSA-GdDTPA concentration was calculated using a phantom with properties similar to those of tumor tissue (25) made from Sephadex-100 with BSA-GdDTPA concentrations in the range 0–0.5 mg/ml, $\ln(S/S_0) = a \times \ln([\text{BSA-GdDTPA}] + b) + c$, with $a = 0.46 \pm 0.06$, $b = 0.024 \pm 0.009$, and $c = 1.71 \pm 0.06$ (values ± SE; $r^2 = 0.995$), where S_0 is signal intensity from the phantom with no added BSA-GdDTPA, and [BSA-GdDTPA] is in mg/ml. A series of 20 spin-echo images acquired during 10 min after administration of BSA-GdDTPA were converted to BSA-GdDTPA concentration maps using this calibration curve. The series of maps were analyzed using the fitting routine within Image Browser 6.1 (Varian) to determine D_0 and D_1, according to Eq. 1. Poorly fit pixels (those with $r^2 < 0.6$) were not included in the analysis. The GdDTPA inflow measurements showed that some tumors had poorly perfused centers, for which perfusion was not well characterized. Therefore, a 20-pixel-wide band in the periphery of all tumors was used in the analysis.

^{31}P Spectra and P_i/NTP Ratios. Localized ^{31}P spectra of the tumor and underlying muscle tissue were obtained (5). Typically, 128 summed free induction decays, acquired into 11,968 data points, were collected from voxels of dimensions 6 × 12 × 12 mm. Spectra were referenced to the resonance of phosphocreatine at 0 ppm. Areas under peaks were integrated for calculation of P_i/NTP ratios.

Analysis of GdDTPA Inflow Data. Initial-rate maps were calculated by subtraction of the sum of three images obtained immediately before injection of GdDTPA from the sum of three images collected immediately after injection of GdDTPA (at t = 15, 45, and 75 s). Alteration to perfusion was also assessed by integrating the curve obtained by plotting the mean signal intensity in a 20-pixel-wide band in the tumor periphery against time after injection of contrast agent, for the inflow experiments made before and 3 h after treatment with CA4P. Maps of T_u and T_c, time constants for uptake and clearance of GdDTPA as defined by Kennedy *et al.* (5, 22), were generated from GdDTPA inflow experiments conducted before and 3 h after CA4P treatment. Briefly, changes in the paramagnetic contribution to the longitudinal relaxation rate (R_{1p}), which is proportional to the concentration of the contrast agent, were fit, on a pixel-by-pixel basis, to Eq. 2 to give T_u and T_c. C_0 is a constant (22):

$$R_{1p}(t) = C_0(1 - e^{-t/T_u})e^{-t/(T_u+T_c)} \quad \text{(B)}$$

RESULTS

Localized ^{31}P spectra were acquired before and until ~3 h after administration of CA4P (Fig. 1). The absence of a signal attributable to phosphocreatine in the spectra of RIF-1 tumors indicated that localized spectra were not contaminated with signal from underlying muscle. A significant decrease in levels of total NTP with a concomitant increase in P_i was seen during this period for two tumor lines, LoVo and RIF-1, which were consequently judged susceptible to CA4P (Fig. 1). A smaller, but significant, alteration in P_i/NTP levels was seen for the SaS and SaF tumors, which were considered to respond relatively poorly to CA4P, whereas no significant change in P_i/NTP level occurred during this period for the HT29 tumor (Fig. 1).

Changes to the perfusion of the tumors were seen which were in accord with the results from ^{31}P MRS. Maps of initial rate of inflow of GdDTPA acquired 3 h after CA4P administration (Fig. 2) showed complete loss of perfusion in as much as 50% of the area of the slices observed in the SaF and RIF-1 tumors. The integral of the curve of mean peripheral pixel intensity after GdDTPA administration showed a significant decrease 3 h after CA4P treatment relative to pretreatment values for LoVo, RIF-1, and SaS but not for SaF and HT29 ($P < 0.05$, Mann-Whitney test; Table 1). The kinetics of inflow and outflow of contrast agent were analyzed on a pixel-by-pixel basis to give values of the uptake (T_u) and clearance (T_c) time constants for each tumor type, before and 3 h after tumor treatment (Table 1). There was no change in T_u for HT29 tumors, but there was a trend of increased T_u for the other tumor types (the differences in T_u were not statistically significant). T_c was not calculated accurately because the values of the time constant for clearance were greater than the 10-min period of acquisition of images.

Experiments made with the RIF-1 tumor implanted into both C3H and SCID mice indicated that there was no significant difference between the tumors grown in the two hosts, in terms of their energetic status, perfusion, or the responses of tumors to treatment with CA4P (data not shown). Anesthesia is known to affect blood pressure in mice, and this could affect both perfusion of the tumors and their energetic status, as determined by ^{31}P MRS, and the response of these parameters to CA4P treatment (26). However, no significant changes in the ^{31}P-containing tumor metabolite levels were observed over a period of 5 h in six SaF tumors, in which the mice were injected with saline instead of CA4P (Fig. 1). There were also no changes in perfusion as determined from measurements of GdDTPA inflow (data

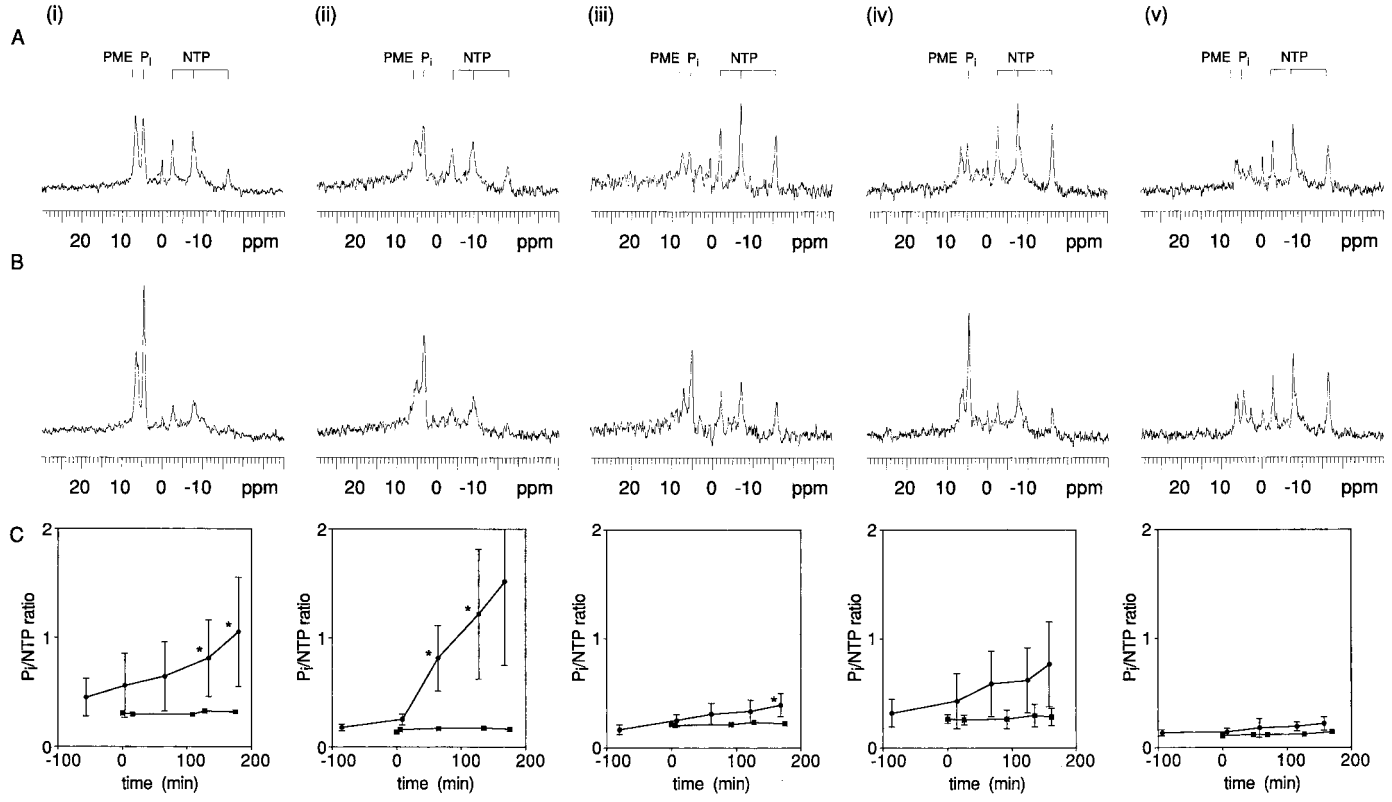

Fig. 1. Localized ^{31}P spectra acquired *A* before and *B* 3 h after CA4P treatment. *C*, ratios of P_i/NTP during this time period (●, $n = 6$ CA4P-treated tumors; ■, $n = 1$ control tumors except SaF where $n = 6$; error bars are ± 1 SD) for five tumor models. For the combretastatin-susceptible tumors, LoVo (*i*) and RIF-1 (*ii*), the signals from the $\alpha-$, $\beta-$, and $\gamma-$phosphates of NTP fall, and the signal from P_i rises. P_i/NTP is not affected to the same extent in SaS (*iii*) and SaF (*iv*) tumors, and no significant change occurs for HT29 (*v*). No significant changes to P_i/NTP ratio are seen in control experiments. Significant differences between the ratio of P_i/NTP before treatment and after treatment: ∗, $P < 0.05$; Mann-Whitney test. PME = phosphate monoesters, predominantly phosphocholine and phosphoethanolamine (30).

not shown). This was confirmed for the other mouse strains and tumors used in this study, where a single animal was used in each case. The results for SCID mice (LoVo and HT29 tumors) indicate that if there are any changes in systemic blood pressure, brought about by CA4P administration, their effect on tumor perfusion and energetic status are relatively small when compared with the direct effect of the drug on tumor vasculature.

Vascular volume fraction and permeability, represented by the parameters D_0 and D_1, respectively (25), were obtained from analysis of BSA-GdDTPA inflow data. D_1 values were significantly higher for LoVo and RIF-1 tumors than they were for SaS and HT29 tumors ($P < 0.05$, Mann-Whitney test; Table 1). D_0 values for HT29 tumors were significantly lower than those of LoVo and RIF-1 tumors ($P < 0.05$, Mann-Whitney test) but not of the other tumors. A correlation was found between vascular permeability, determined as D_1, and the response of the five tumor

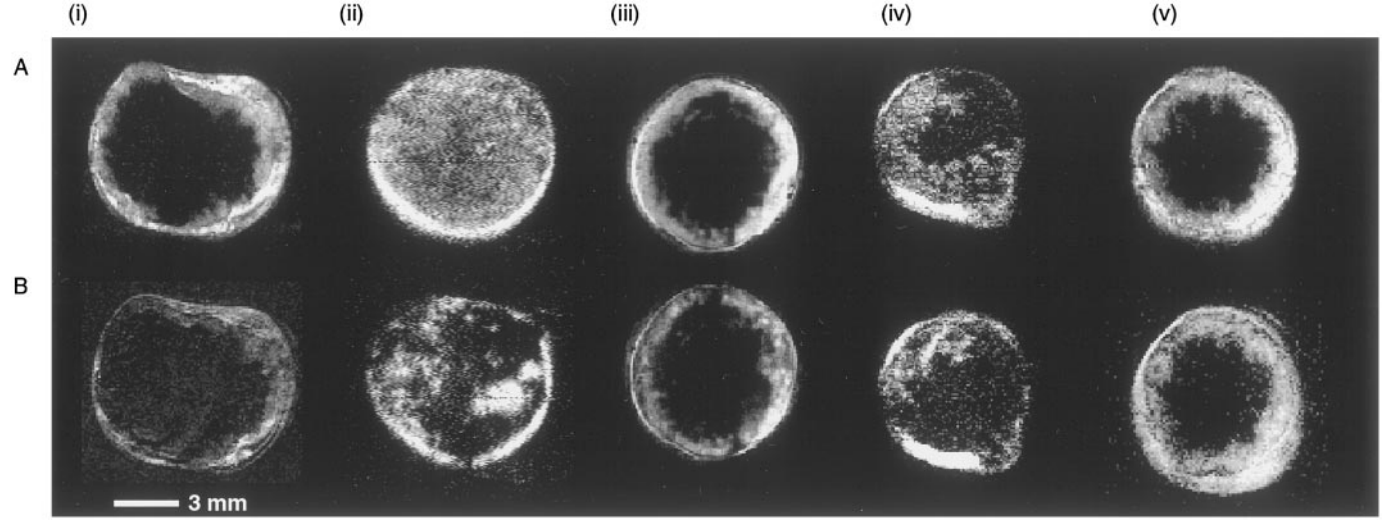

Fig. 2. Tumor perfusion assessed using initial rate of inflow of GdDTPA for the five tumor models. Images are pre- (*A*) and 3 h post- (*B*) CA4P treatment. Loss in signal intensity, corresponding to a reduction in perfusion, is seen for LoVo (*i*) and RIF-1 (*ii*) tumors, whereas this occurs to a lesser extent in SaS (*iii*), SaF (*iv*), and HT29 (*v*) tumors.

Table 1 *Analysis of BSA-GdDTPA and GdDTPA inflow data*
Values are mean ± 1 s.d., for $n = 6$ animals in all cases.

	LoVo	RIF-1	SaS	SaF	HT29
D_0 (mg/ml)[a]	0.058 ± 0.006	0.048 ± 0.002	0.046 ± 0.007	0.037 ± 0.001	0.033 ± 0.002*
D_1 (mg/ml/s)[a]	0.0027 ± 0.0004*	0.004 ± 0.001*	0.0017 ± 0.0002	0.0022 ± 0.0003	0.0017 ± 0.0002
post/pretreatment ratio[b]	0.50 ± 0.04*	0.5 ± 0.1*	0.5 ± 0.1*	0.7 ± 0.2	0.9 ± 0.1
T_u (pretreatment) (s)[c]	180 ± 70	140 ± 80	140 ± 40	120 ± 50	300 ± 60
T_u (posttreatment) (s)[c]	300 ± 100	310 ± 90	250 ± 40	210 ± 60	320 ± 80

[a] BSA-GdDTPA inflow data reports on vessel permeability; D_0 and D_1 are related to vascular volume fraction and permeability (* : D_0 of HT29 is significantly different from both LoVo and RIF-1; D_1 of both LoVo and RIF-1 are significantly different from each of SaS and HT29: $P < 0.05$, Mann-Whitney test).
[b] The integral of the uptake curve of signal intensities after GdDTPA administration was determined before and 3 h after CA4P treatment as a measure of bulk perfusion. The ratio of these integrals (post-/pre-) indicates the change in perfusion post-treatment. This was altered except in the case of SaF and HT29 (* : $P < 0.05$, Mann-Whitney test).
[c] Time constants for uptake (T_u) and clearance (T_c) of GdDTPA.

models used in the study to CA4P, measured as P_i/NTP ratio 3 h after treatment (Fig. 3).

DISCUSSION

Combretastatin A4 and its soluble prodrug cause rapid and selective disruption of tumor vasculature (2, 4, 5). This was proposed to be the result of the activity of CA4P against recently divided endothelial cells (2). Because VEGF is one of the main growth factors responsible for stimulating endothelial cell proliferation in tumors (8), and the level of this growth factor has been shown to correlate with vascular permeability measured using MRI (12–17), we set out to determine whether there was a correlation between vessel permeability and susceptibility to the drug.

Vascular permeability was assessed using the pharmacokinetic model of Su *et al.* (Ref. 25; Table 1). The larger D_1 values for the LoVo and RIF-1 tumors indicated that the transport constant (K_1) was greater in these tumors than in the SaS, SaF, and HT29 tumors, indicative of greater vessel permeability. The D_0 value for the HT29 tumor was significantly lower than that of the LoVo and RIF-1 tumors, indicative of lower vascular volume fraction in this tumor, but was not significantly different from that of the SaS and SaF tumors. The variations in D_1 and D_0 did not correlate with tumor growth rate, as both RIF1 and LoVo tumors had relatively permeable vasculature and relatively high vascular volume fraction, yet grew at rates which were very different (geometric mean diameter of 10 mm was attained 11–16 and 50–60 days after implantation, respectively).

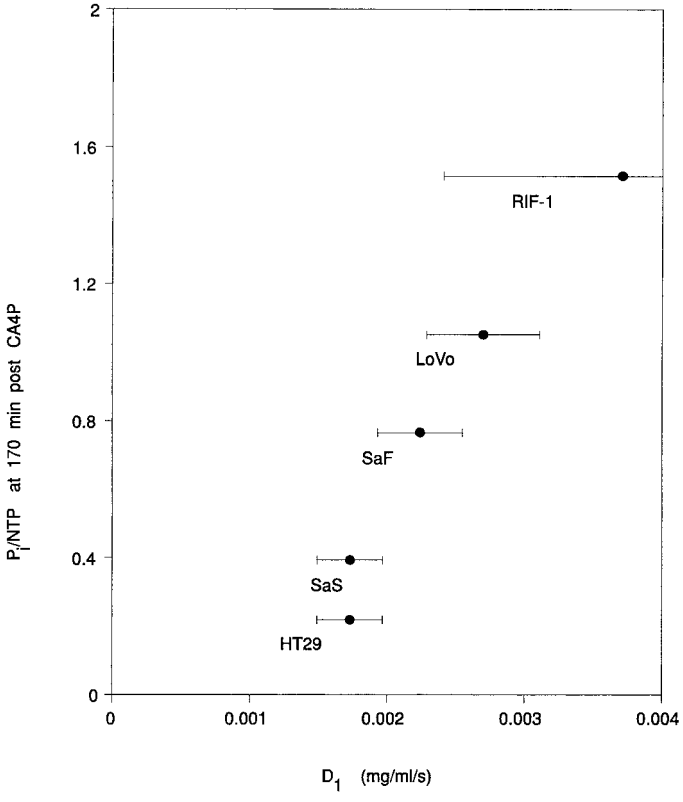

Fig. 3. Vascular permeability (as D_1) of five tumor models is correlated with response to CA4P treatment, taken as the P_i/NTP ratio 3 h after treatment.

Responsiveness of tumors to treatment was assessed using two criteria. The most sensitive technique for assessing response was found to be ^{31}P MRS. LoVo and RIF-1 were classed as responsive tumors because localized ^{31}P spectroscopy showed a significant increase in P_i/NTP ratio within 3 h (Fig. 1), indicating that tumor cells were subject to hypoxia and/or hypoglycemia after systemic treatment with CA4P. A reduced response was seen for SaS and SaF, and no significant changes in P_i/NTP ratio were seen in the HT29 tumor.

The response of tumors to CA4P was also assessed on the basis of changes to perfusion 3 h after treatment. The clearest indicator of altered perfusion was the initial-rate map (Fig. 2), which highlighted the parts of the tumor in which perfusion was reduced. This was also evident when the integral of the curve obtained by plotting signal intensity against time during GdDTPA inflow was calculated. This may be taken as a measure of bulk perfusion, and significant decreases were seen for all tumor types, except for HT29. A more complete analysis of the rate constants of uptake and clearance of GdDTPA (22) indicated that the rate of inflow of GdDTPA (T_u) into all tumors except for HT29 was decreased, 3 h after CA4P treatment (Table 1). However, the initial-rate maps illustrate that the vascular disruption caused by CA4P results primarily in loss of perfusion to regions of the tumor, rather than in a reduction of the overall rate of perfusion in the tumor. This was supported by the fact that the increase in T_u in the tumors was not statistically significant. As was the case for ^{31}P MRS, these analyses indicated that LoVo and RIF-1 tumors respond more to CA4P treatment than do SaS, SaF, and HT29 tumors. Whereas the primary result of CA4P treatment is reduced perfusion, as determined using these MRI experiments, the secondary effect of damage to tumor cells is measured in the ^{31}P MRS experiments. A direct relationship between the two assessments of tumor response to CA4P would not necessarily be expected. Furthermore, the ^{31}P MRS experiment interrogates the whole of the tumor, whereas in the imaging experiments performed here, only the selected slice was observed. In the clinic, investigation of alterations to perfusion is likely to be routinely possible, whereas hardware for ^{31}P MRS is less widespread.

The lack of response to CA4P treatment of the HT29 tumor could not be ascribed to properties of the SCID mouse host. Two other tumors were implanted into SCID mice, LoVo and RIF-1, both of which responded well to CA4P treatment. No significant differences were seen between RIF-1 tumors borne by SCID and C3H hosts in

terms of perfusion, energetic status, or the responses of these to treatment with CA4P (data not shown).

The correlation between MRI measurements of vessel permeability, which has been shown to be a surrogate marker for VEGF expression (12–17), and the susceptibility of the tumors to CA4P (Fig. 3) accords with the expectation that angiogenic tumors, with higher levels of endothelial cell proliferation, will be more susceptible to the drug. This correlation is reinforced by the observation that there is also a correlation, albeit weaker, between drug susceptibility and vascular volume. The vascular volume of the unresponsive HT29 tumor was significantly lower then the vascular volumes of the LoVo and RIF-1 tumors, which responded well to the drug. Vascular volume, like permeability, is considered a reasonable surrogate marker of angiogenesis (27), and MRI measurements of vascular volume have been shown to correlate with VEGF-induced angiogenesis (14). However, the control of vessel permeability is complex, and it is possible that other growth factors may also play an important role (8, 28).

These experiments suggest that macromolecular contrast agents could be used in the clinic to assess permeability of tumor vasculature, as a possible indicator of the likelihood of response of tumors to CA4P. Macromolecular contrast agents other than those based on albumin-GdDTPA, *e.g.*, the superparamagnetic iron oxide particle-containing agents (29), may be suitable for such measurements.

ACKNOWLEDGMENTS

We thank the Cancer Research Campaign for project grants, Chris Price and Simon Williams for help with setting up the fitting routines, and G. R. Pettit for kindly providing CA4P.

REFERENCES

1. Pettit, G. R., Singh, S. B., Hamel, E., Lin, C. M., Alberts, D. S., and Garcia-Kendall, D. Isolation and structure of the strong cell growth and tubulin inhibitor combretastatin A-4. Experientia, *45:* 115–211, 1989.
2. Dark, G. G., Hill, S. A., Prise, V. E., Tozer, G. M., Pettit, G. R., and Chaplin, D. J. Combretastatin A-4, an agent that displays potent and selective toxicity toward tumor vasculature. Cancer Res., *57:* 1829–1834, 1997.
3. Rustin, G., Galbraith, S., Taylor, N., Maxwell, R., Tozer, G., Baddeley, H., Wilson, I., and Prise, V. Combretastatin A4 phosphate (CA4P) selectively targets vasculature in animal and human tumors. Clin. Cancer Res., *5:* 14S, 1999.
4. Iyer, S., Chaplin, D. J., Rosenthal, D. S., Boulares, A. H., Li, L-Y., and Smulson, M. E. Induction of apoptosis in proliferating human endothelial cells by the tumor-specific agent combretastatin A-4. Cancer Res., *58:* 4510–4514, 1998.
5. Beauregard, D. A., Thelwall, P. E., Chaplin, D. J., Hill, S. A., Adams, G. E., and Brindle, K. M. Magnetic resonance imaging and spectroscopy of combretastatin A_4 prodrug-induced disruption of tumour perfusion and energetic status. Br. J. Cancer, *77:* 1761–1767, 1998.
6. Parkins, C., Holder, A., Hill, S., Chaplin, D., and Tozer, G. Determinants of anti-vascular action by combretastatin A-4 phosphate: role of nitric oxide. Br. J. Cancer, *83:* 811–816, 2000.
7. Tozer, G. M., Prise, V. E., Wilson, J., Locke, R. J., Vojnovic, B., Stratford, M. R. L., Dennis, M. F., and Chaplin, D. J. Combretastatin A-4 phosphate as a tumor vascular-targeting agent: early effects in tumors and normal tissues. Cancer Res., *59:* 1626–1634, 1999.
8. Carmeliet, P., and Jain, R. K. Angiogenesis in cancer and other diseases. Nature (Lond.), *407:* 249–257, 2000.
9. Chaplin, D. J., Pettit, G. R., and Hill, S. A. Anti-vascular approaches to solid tumour therapy: evaluation of combretastatin A4 phosphate. Anticancer Res., *19:* 189–195, 1999.
10. Galbraith, S., Taylor, N., Maxwell, R., Lodge, M., Tozer, G., Baddeley, H., Wilson, I., Prise, V., and Rustin, G. Combretastatin A4 phosphate (CA4P) targets vasculature in animal and human tumours. Br. J. Cancer, *83:* 17S1, 2000.
11. Furman-Haran, E., Margalit, R., Grobgeld, D., and Degani, H. Dynamic contrast-enhanced magnetic resonance imaging reveals stress-induced angiogenesis in MCF7 human breast tumours. Proc. Natl. Acad. Sci. USA, *93:* 6247–6251, 1996.
12. Brasch, R., Pham, C., Shames, D., Roberts, T., van Dijke, K., van Bruggen, N., Mann, J., Ostrowitzki, S., and Melnyk, O. Assessing tumor angiogenesis using macromolecular MR imaging contrast media. J. Magn. Reson. Imaging, *7:* 68–74, 1997.
13. Pham, C., Roberts, T., van Bruggen, N., Melnyk, O., Mann, J., Ferrara, N., Cohen, R., and Brasch, R. Magnetic resonance imaging detects suppression of tumor vascular permeability after administration of antibody to vascular endothelial growth factor. Cancer Investig., *16:* 225–230, 1998.
14. Lewin, M., Bredow, S., Serveyev, N., Marecos, E., Bogdanov, A., Jr., and Weissleder, R. *In vivo* assessment of vascular endothelial growth factor-induced angiogenesis. Int. J. Cancer, *83:* 798–802, 1999.
15. Abramovitch, R., Dafni, H., Smouha, E., Benjamin, L. E., and Neeman, M. *In vivo* prediction of vascular susceptibility to vascular endothelial growth factor withdrawal: magnetic resonance imaging of C6 rat glioma in nude mice. Cancer Res., *59:* 5012–5016, 1999.
16. Bhujwalla, Z., Artemov, D., and Solaiyappan, M. Insights into tumor vascularization using magnetic resonance imaging and spectroscopy. Exp. Oncol., *22:* 3–7, 2000.
17. Brasch, R., and Turetschek, K. MRI characterization of tumors and grading angiogenesis using macromolecular contrast media: status report. Eur. J. Radiol., *34:* 148–155, 2000.
18. Twentyman, P. R., Brown, J. M., Gray, J. W., Franko, A. J., Scoles, M. A., and Kallman, R. F. A new mouse tumor model system (RIF-1) for comparison of end-point studies. J. Natl. Cancer Inst. (Bethesda), *64:* 595–604, 1980.
19. Denekamp, J., Hill, S. A., and Hobson, B. Vascular occlusion and tumour cell death. Eur. J. Cancer Clin. Oncol., *19:* 271–275, 1983.
20. Pettit, G. R., Temple, C., Narayanan, V. L., Varma, R., Simpson, M. J., Boyd, M. R., Rener, G. A., and Bansal, N. Antineoplastic agents 322. Synthesis of combretastatin A-4 prodrugs. Anticancer Drug Des., *10*: 299–309, 1995.
21. Ogan, M. D., Schmiedl, U., Moseley, M. E., Grodd, W., Paajanen, H., and Brasch, R. C. Albumin labeled with Gd-DTPA. An intravascular contrast-enhancing agent for magnetic resonance blood pool imaging: preparation and characterization. Investig. Radiol., *22:* 665–671, 1987.
22. Kennedy, S. D., Szczepaniak, L. S., Gibson, S. L., Hilf, R., Foster, T. H., and Bryant, R. G. Quantitative MRI of Gd-DTPA uptake in tumours: response to photodynamic therapy. Magn. Reson. Med., *31:* 292–301, 1994.
23. Schmiedl, U., Ogan, M., Paajanen, H., Marotti, M., Crooks, L. E., Brito, A. C., and Brasch, R. C. Albumin labeled with Gd-DTPA as an intravascular, blood pool-enhancing agent for MR imaging: biodistribution and imaging studies. Radiology, *162:* 205–210, 1987.
24. Daldrup, H., Shames, D. M., Wendland, M., Okuhata, Y., Link, T. M., Rosenau, W., Lu, Y., and Brasch, R. C. Correlation of dynamic contrast-enhanced magnetic resonance imaging with histologic tumor grade: comparison of macromolecular and small-molecule contrast media. Pediatr. Radiol., *28:* 67–78, 1998.
25. Su, M-Y., Jao, J-C., and Nalcioglu, O. Measurement of vascular volume fraction and blood-tissue permeability constants with a pharmacokinetic model: studies in rat muscle tumors with dynamic Gd-DTPA enhanced MRI. Magn. Reson. Med., *32:* 714–724, 1994.
26. Wood, P. J., Sansom, J. M., Stratford, I. J., Adams, G. E., Szabo, C., Thiemermann, C., and Vane, J. R. Modification of metabolism of transplantable and spontaneous murine tumors by the nitric oxide synthase inhibitor, nitro-L-arginine. Int. J. Radiat. Oncol. Biol. Phys., *29:* 443–447, 1994.
27. Jain, R. Determinants of tumor blood flow: a review. Cancer Res., *48:* 2641–2658, 1988.
28. Clauss, M., Sunderkötter, C., Sveinbjörnsson, B., Hippenstiel, S., Willuweit, A., Marino, M., Haas, E., Seljelid, R., Scheurich, P., Suttorp, N., Grell, M., and Risau, W. A permissive role for tumor necrosis factor in vascular endothelial growth factor-induced vascular permeability. Blood, *97:* 1321–1329, 2001.
29. Taylor, A., Panting, J., Keegan, J., Gatehouse, P., Amin, D., Jhooti, P., Yang, G., McGill, S., Burman, E., Francis, J., Firmin, D., and Pennell, D. Safety and preliminary findings with the intravascular contrast agent NC100150 injection for MR coronary angiography. J. Magn. Reson. Imaging, *9:* 220–227, 1999.
30. Bhujwalla, Z. M., Shungu, D. C., He, Q., Wehrle, J. P., and Glickson, J. D. MR studies of tumours: relationship between blood flow, metabolism, and physiology. *In:* R. J. Gillies (ed.), NMR in Physiology and Biomedicine, pp. 311–328. San Diego, CA: Academic Press, Inc., 1994.